# Exposing Digital Forgeries Through Chromatic Aberration

Micah K. Johnson
Department of Computer Science
Dartmouth College
Hanover, NH 03755
kimo@cs.dartmouth.edu

Hany Farid
Department of Computer Science
Dartmouth College
Hanover, NH 03755
farid@cs.dartmouth.edu

## ABSTRACT

Virtually all optical imaging systems introduce a variety of aberrations into an image. Chromatic aberration, for example, results from the failure of an optical system to perfectly focus light of different wavelengths. Lateral chromatic aberration manifests itself, to a first-order approximation, as an expansion/contraction of color channels with respect to one another. When tampering with an image, this aberration is often disturbed and fails to be consistent across the image. We describe a computational technique for automatically estimating lateral chromatic aberration and show its efficacy in detecting digital tampering.

## Categories and Subject Descriptors

I.4 [**Image Processing**]: Miscellaneous

## General Terms

Security

## Keywords

Digital Tampering, Digital Forensics

## 1. INTRODUCTION

Most images contain a variety of aberrations that result from imperfections and artifacts of the optical imaging system. In an ideal imaging system, light passes through the lens and is focused to a single point on the sensor. Optical systems, however, deviate from such ideal models in that they fail to perfectly focus light of all wavelengths. The resulting effect is known as chromatic aberration which occurs in two forms: longitudinal and lateral. Longitudinal aberration manifests itself as differences in the focal planes for different wavelengths of light. Lateral aberration manifests itself as a spatial shift in the locations where light of different wavelengths reach the sensor – this shift is proportional to the distance from the optical center. In both

cases, chromatic aberration leads to various forms of color imperfections in the image. To a first-order approximation, longitudinal aberration can be modeled as a convolution of the individual color channels with an appropriate low-pass filter. Lateral aberration, on the other hand, can be modeled as an expansion/contraction of the color channels with respect to one another. When tampering with an image, these aberrations are often disturbed and fail to be consistent across the image.

We describe a computational technique for automatically estimating lateral chromatic aberration. Although we eventually plan to incorporate longitudinal chromatic aberration, only lateral chromatic aberration is considered here. We show the efficacy of this approach for detecting digital tampering in synthetic and real images. This work provides another tool in a growing number of image forensic tools, [3, 7, 8, 10, 9, 5, 6].

## 2. CHROMATIC ABERRATION

We describe the cause of lateral chromatic aberration and derive an expression for modeling it. For purposes of exposition a one-dimensional imaging system is first considered, and then the derivations are extended to two dimensions.

### 2.1 1-D Aberration

In classical optics, the refraction of light at the boundary between two media is described by Snell's Law:

$$n \sin(\theta) = n_f \sin(\theta_f), \qquad (1)$$

where $\theta$ is the angle of incidence, $\theta_f$ is the angle of refraction, and $n$ and $n_f$ are the refractive indices of the media through which the light passes. The refractive index of glass, $n_f$, depends on the wavelength of the light that traverses it. This dependency results in polychromatic light being split according to wavelength as it exits the lens and strikes the sensor. Shown in Figure 1, for example, is a schematic showing the splitting of short wavelength (solid blue ray) and long wavelength (dashed red ray) light. The result of this splitting of light is termed lateral chromatic aberration.

Lateral chromatic aberration can be quantified with a low-parameter model. Consider, for example, the position of short wavelength (solid blue ray) and long wavelength (dashed red ray) light on the sensor, $x_r$ and $x_b$, Figure 1. With no chromatic aberration, these positions would be equal. In the presence of chromatic aberration, it can be shown (Appendix A) that these positions can be modeled as:
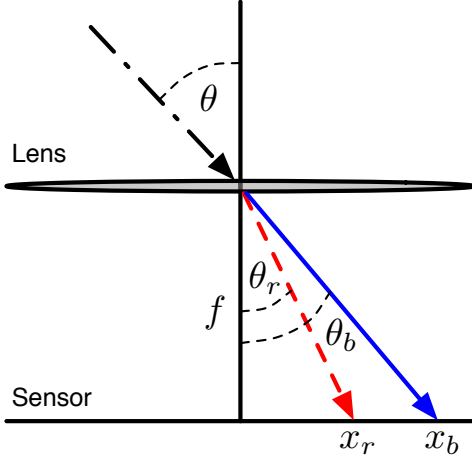
$$x_r \approx \alpha x_b, \qquad (2)$$

**Figure 1: The refraction of light in one dimension. Polychromatic light enters the lens at an angle $\theta$, and emerges at an angle which depends on wavelength. As a result, different wavelengths of light, two of which are represented as the red (dashed) and the blue (solid) rays, will be imaged at different points, $x_r$ and $x_b$.**
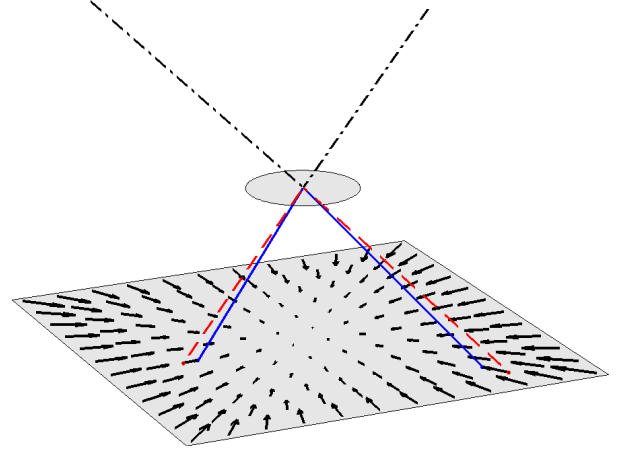


**Figure 2: The refraction of light in two dimensions. Polychromatic light enters the lens and emerges at an angle which depends on wavelength. As a result, different wavelengths of light, two of which are represented as the red (dashed) and the blue (solid) rays, will be imaged at different points. The vector field shows the amount of deviation across the image.**

where $\alpha$ is a scalar value. This model generalizes for any two wavelengths of light, where $\alpha$ is a function of these wavelengths.

## 2.2 2-D Aberration

For a two-dimensional lens and sensor, the distortion caused by lateral chromatic aberration takes a form similar to Equation (2). Consider again the position of short wavelength (solid blue ray) and long wavelength (dashed red ray) light on the sensor, $(x_r, y_r)$ and $(x_b, y_b)$. In the presence of chromatic aberration, it can be shown (Appendix A) that these positions can be modeled as:

$$(x_r, y_r) \quad \approx \quad \alpha(x_b, y_b), \tag{3}$$

where $\alpha$ is a scalar value.

Shown in Figure 2 is vector-based depiction of this aberration, where each vector $\vec{v} = (x_r - x_b, y_r - y_b)$. Note that this model is simply an expansion/contraction about the center of the image. In real lenses, the center of optical aberrations is often different from the image center due to the complexities of multi-lens systems [12]. The previous model can therefore be augmented with an additional two parameters, $(x_0, y_0)$, to describe the position of the expansion/contraction center. The model now takes the form:

$$x_r \quad = \quad \alpha(x_b - x_0) + x_0 \tag{4}$$
$$y_r \quad = \quad \alpha(y_b - y_0) + y_0. \tag{5}$$

It is common for lens designers to try to minimize chromatic aberration in lenses. This is usually done by combining lenses with different refractive indices to align the rays for different wavelengths of light. If two wavelengths are aligned, the lens is called an achromatic doublet or achromat. It is not possible for all wavelengths that traverse an achromatic doublet to be aligned and the residual error is known as the secondary spectrum. The secondary spectrum

is visible in high-contrast regions of an image as a magenta or green halo [4].

## 2.3 Estimating Chromatic Aberration

In the previous section, a model for lateral chromatic aberration was derived, Equations (4)–(5). This model describes the relative positions at which light of varying wavelength strikes the sensor. With a three color channel RGB image, we assume that the lateral chromatic aberration is constant within each color channel. Using the green channel as reference, we would like to estimate the aberration between the red and green channels, and between the blue and green channels. Deviations or inconsistencies in these models will then be used as evidence of tampering.

Recall that the model for lateral chromatic aberration consists of three parameters, two parameters for the center of the distortion and one parameter for the magnitude of the distortion. These model parameters will be denoted $(x_1, y_1, \alpha_1)$ and $(x_2, y_2, \alpha_2)$ for the red to green and blue to green distortions, respectively.

The estimation of these model parameters can be framed as an image registration problem [1]. Specifically, lateral chromatic aberration results in an expansion or contraction between the color channels, and hence a misalignment between the color channels. We, therefore, seek the model parameters that bring the color channels back into alignment. There are several metrics that may be used to quantify the alignment of the color channels. To help contend with the inherent intensity differences across the color channels we employ a metric based on mutual information that has proven successful in such situations [11]. We have found that this metric achieves slightly better results than a simpler correlation coefficient metric (with no difference in the
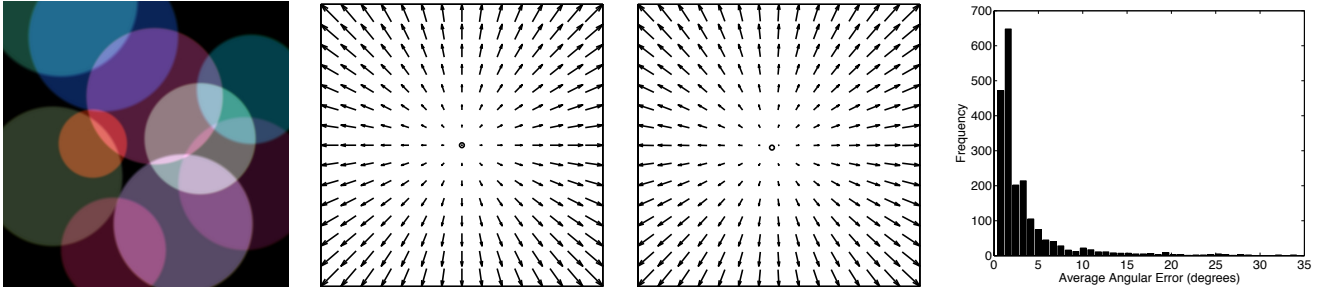
**Figure 3: Synthetically generated images. Shown are, from left to right, a sample image, the distortion applied to the blue channel (the small circle denotes the distortion center), the estimated distortion, and a histogram of angular errors from 2000 images. For purposes of display, the vector fields are scaled by a factor of 50.**

run-time complexity[1]). Other metrics, however, may very well achieve similar or better results.

We will describe the estimation of the red to green distortion parameters (the blue to green estimation follows a similar form). Denote the red channel of a RGB image as $R(x,y)$ and the green channel as $G(x,y)$. A corrected version of the red channel is denoted as $R(x_r, y_r)$ where:

$$x_r = \alpha_1(x - x_1) + x_1 \tag{6}$$
$$y_r = \alpha_1(y - y_1) + y_1 \tag{7}$$

The model parameters are determined by maximizing the mutual information between $R(x_r, y_r)$ and $G(x,y)$ as follows:

$$\text{argmax}_{x_1, y_1, \alpha_1} I(\mathcal{R}; \mathcal{G}), \tag{8}$$

where $\mathcal{R}$ and $\mathcal{G}$ are the random variables from which the pixel intensities of $R(x_r, y_r)$ and $G(x,y)$ are drawn. The mutual information between these random variables is defined to be:

$$I(\mathcal{R}; \mathcal{G}) = \sum_{r \in \mathcal{R}} \sum_{g \in \mathcal{G}} P(r, g) \log \left( \frac{P(r, g)}{P(r)P(g)} \right), \tag{9}$$

where $P(\cdot, \cdot)$ is the joint probability distribution, and $P(\cdot)$ is the marginal probability distribution.

This metric of mutual information is maximized using a brute-force iterative search. On the first iteration, a relatively course sampling of the parameter space for $x_1, y_1, \alpha_1$ is searched. On the second iteration, a refined sampling of the parameter space is performed about the maximum from the first stage. This process is repeated for $N$ iterations. While this brute-force search can be computationally demanding, it does ensure that the global minimum is reached. Standard gradient descent optimization techniques may be employed to improve run-time complexity.

In order to quantify the error between the estimated and known model parameters, we compute the average angular error between the displacement vectors at every pixel. Specifically, let $x_0, y_0, \alpha_0$ be the actual parameters and let $x_1, y_1, \alpha_1$ be the estimated model parameters. The vector

---

[1]The run-time complexity is dominated by the interpolation necessary to generate $R(x_r, y_r)$, and not the computation of mutual information.

displacement fields for these distortions are:

$$\vec{v}_0(x,y) = \begin{pmatrix} (\alpha_0(x - x_0) + x_0) - x \\ (\alpha_0(y - y_0) + y_0) - y \end{pmatrix} \tag{10}$$

$$\vec{v}_1(x,y) = \begin{pmatrix} (\alpha_1(x - x_1) + x_1) - x \\ (\alpha_1(y - y_1) + y_1) - y \end{pmatrix} \tag{11}$$

The angular error $\theta(x,y)$ between any two vectors is:

$$\theta(x,y) = \cos^{-1} \left( \frac{\vec{v}_0(x,y) \cdot \vec{v}_1(x,y)}{||\vec{v}_0(x,y)|| \, ||\vec{v}_1(x,y)||} \right). \tag{12}$$

The average angular error, $\bar{\theta}$, over all $P$ pixels in the image is:

$$\bar{\theta} = \frac{1}{P} \sum_{x,y} \theta(x,y). \tag{13}$$

To improve reliability, this average is restricted to vectors whose norms are larger than a specified threshold, 0.01 pixels. It is this measure, $\bar{\theta}$, that is used to quantify the error in estimating lateral chromatic aberration.

## 3. RESULTS

We demonstrate the suitability of the proposed model for lateral chromatic aberration, and the efficacy of estimating this aberration using the mutual information-based algorithm. We first present results from synthetically generated images. Results are then presented for a set of calibrated images photographed under different lenses and lens settings. We also show how inconsistencies in lateral chromatic aberration can be used to detect tampering in visually plausible forgeries.

### 3.1 Synthetic images

Synthetic color images of size $512 \times 512$ were generated as follows. Each image consisted of ten randomly placed anti-aliased discs of various sizes and colors, Figure 3. Lateral chromatic aberration was simulated by warping the blue channel relative to the green channel. The center of the distortion, $x_2, y_2$, was the image center, and the distortion coefficient, $\alpha_2$, was chosen between 1.0004 and 1.0078, producing maximum displacements of between 0.1 and 2 pixels. Fifty random images for each of forty values of $\alpha_2$ were generated for a total of 2000 images.

As described in the previous section, the distortion parameters are determined by maximizing the mutual information,

Equation (9), for the blue to green distortion. On the first iteration of the brute-force search algorithm, values of $x_2, y_2$ spanning the entire image were considered, and values of $\alpha_2$ between 1.0002 to 1.02 were considered. Nine iterations of the search algorithm were performed, with the search space consecutively refined on each iteration.

Shown in the second and third panels of Figure 3 are examples of the applied and estimated distortion (the small circle denotes the distortion center). Shown in the fourth panel of Figure 3 is the distribution of average angular errors from 2000 images. The average error is 3.4 degrees with 93% of the errors less than 10 degrees. These results demonstrate the general efficacy of the mutual information-based algorithm for estimating lateral chromatic aberration.

## 3.2 Calibrated images

In order to test the efficacy of our approach on real images, we first estimated the lateral chromatic aberration for two lenses at various focal lengths and apertures. A 6.3 mega-pixel Nikon D-100 digital camera was equipped with a Nikkor 18–35mm ED lens and a Nikkor 70–300mm ED lens[2]. For the 18–35 mm lens, focal lengths of 18, 24, 28, and 35 mm with 17 $f$-stops, ranging from $f/29$ to $f/3.5$, per focal length were considered. For the 70–300 mm lens, focal lengths of 70, 100, 135, 200, and 300 with 19 $f$-stops, ranging from $f/45$ to $f/4$, per focal length were considered.

A calibration target was constructed of a peg board with 1/4-inch diameter holes spaced one inch apart. The camera was positioned at a distance from the target so that roughly 500 holes appeared in each image. This target was back-illuminated with diffuse lighting, and photographed with each lens and lens setting described above. For each color channel of each calibration image, the center of the holes were automatically computed with sub-pixel resolution. The red to green lateral chromatic aberration was estimated by comparing the relative positions of these centers across the entire image. The displacements between the centers were then modeled as a three parameter expansion/contraction pattern, $x_1, y_1, \alpha_1$. These parameters were estimated using a brute force search that minimized the root mean square error between the measured displacements and the model. Shown in the top panel of Figure 4 is the actual red to green distortion, and shown in the bottom panel is the best model fit. Note that while not perfect, the three parameter model is a reasonable approximation to the actual distortion. The blue to green aberration was estimated in a similar manner, yielding model parameters $x_2, y_2, \alpha_2$. This calibration data was used to quantify the estimation errors from real images of natural scenes.

Images of natural scenes were obtained using the same camera and calibrated lenses. These images, of size $3020 \times 2008$ pixels, were captured and stored in uncompressed TIFF format (see below for the effects of JPEG compression). For each of the 205 images, the focal length and $f$-stop were extracted from the EXIF data in the image header. The estimated aberration from each image was then compared with the corresponding calibration data with the same lens settings.

The distortion parameters were determined by maximizing the mutual information, Equation (9), between the red and green, and blue and green channels. On the first itera-

---

[2]ED lenses help to eliminate secondary chromatic aberration.
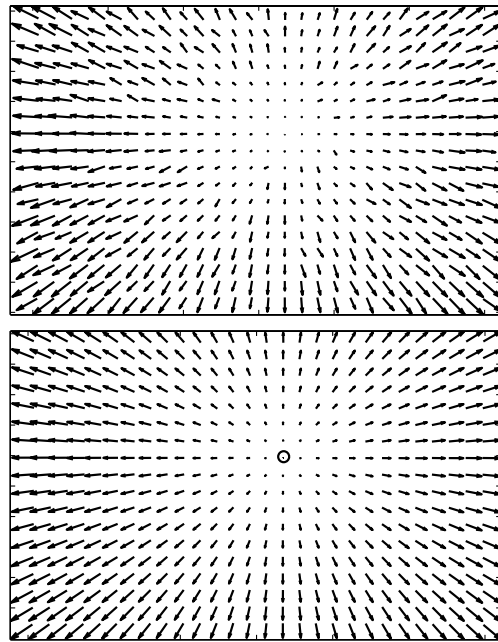


**Figure 4: Calibration. Shown in the top panel is an actual red to green chromatic aberration. Shown in the bottom panel is the best three parameter model fit to this distortion. Note that the actual distortion is well fit by this model. For purposes of display, the vector fields are scaled by a factor of** 100.

tion of the brute-force search algorithm, values of $x_1, y_1$ and $x_2, y_2$ spanning the entire image were considered, and values of $\alpha_1$ and $\alpha_2$ between 0.9985 to 1.0015 were considered. The bounds on $\alpha_1$ and $\alpha_2$ were chosen to include the entire range of the distortion coefficient measured during calibration, 0.9987 to 1.0009. Nine iterations of the search algorithm were performed, with the search space consecutively refined on each iteration.

Shown in the top panel of Figure 5 is one of the 205 images. Shown in the second and third panels are the calibrated and estimated blue to green distortions (the small circle denotes the distortion center). Shown in the bottom panel of Figure 5 is the distribution of average angular errors, Equation (13), from the red to green and blue to green distortions from all 205 images. The average error is 20.3 degrees with 96.6% of the errors less than 60 degrees. Note that the average errors here are approximately six times larger than the synthetically generated images of the previous section. Much of the error is due to other aberrations in the images, such as longitudinal aberration, that are not considered in our current model.

### 3.2.1 JPEG Compression

The results of the previous section were based on uncompressed TIFF format images. Here we explore the effect of lossy JPEG compression on the estimation of chromatic aberration. Each of the 205 uncompressed images described in the previous section were compressed with a JPEG quality of 95, 85, and 75 (on a scale of 1 to 100). The chromatic aberration was estimated as described above, and the same
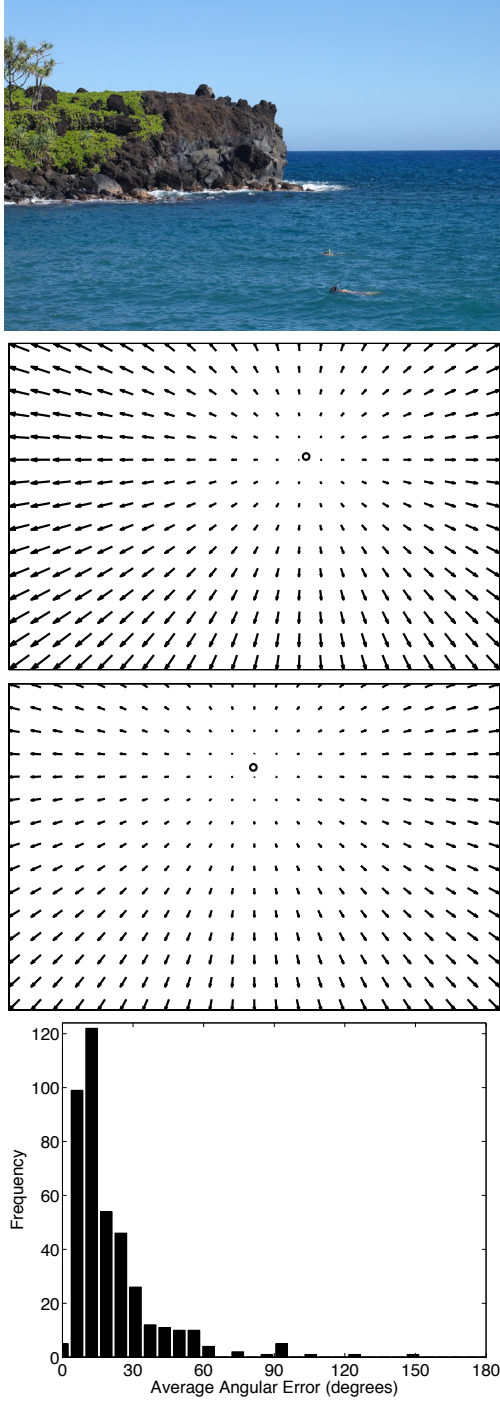
**Figure 5: Calibrated images. Shown are, from top to bottom, one of the 205 images, the calibrated blue to green aberration, the estimated aberration, and a histogram of angular errors from 205 images, for the blue to green and red to green aberrations. For purposes of display, the vector fields are scaled by a factor of 150.**

error metric computed. For a quality of 95, the average error was 26.1 degrees with 93.7% of the errors less than 60 degrees. For a quality of 85, the average error was 26.7 degrees with 93.4% of the errors less than 60 degrees. For a quality of 75, the average error was 28.9 degrees with 93.2% of the errors less than 60 degrees. These errors should be compared to the uncompressed images with an average error of 20.3 degrees and with 96.6% of the errors less than 60 degrees. While the estimation suffers a bit, it is still possible to estimate, with a reasonable amount of accuracy, chromatic aberration from JPEG compressed images

## 3.3 Forensics

When creating a forgery, it is sometimes necessary to conceal a part of an image with another part of the image or to move an object from one part of an image to another part of an image. These types of manipulations will lead to inconsistencies in the lateral chromatic aberrations, which can therefore be used as evidence of tampering.

In order to detect tampering based on inconsistent chromatic aberration, it is first assumed that only a relatively small portion of an image has been manipulated. With the additional assumption that this manipulation will not significantly affect a global estimate, the aberration is estimated from the entire image. This global estimate is then compared against estimates from small blocks. Any block that deviates significantly from the global estimate is suspected of having been manipulated.

The 205 calibrated images described in the previous section were each partitioned into overlapping $300 \times 300$ pixels blocks. It is difficult to estimate chromatic aberration from a block with little or no spatial frequency content (e.g., a largely uniform patch of sky). As such, the average gradient for each image block was computed and only 50 blocks with the largest gradients were considered. The gradient, $\nabla I(x, y)$, is computed as follows:

$$\nabla I(x,y) \quad = \quad \sqrt{I_x^2(x,y) + I_y^2(x,y)}, \qquad (14)$$

where $I_x(\cdot)$ and $I_y(\cdot)$ are the horizontal and vertical partial derivatives estimated as follows:

$$I_x(x,y) \quad = \quad (I(x,y) \star d(x)) \star p(y) \qquad (15)$$
$$I_y(x,y) \quad = \quad (I(x,y) \star d(y)) \star p(x), \qquad (16)$$

where $\star$ denotes convolution and $d(\cdot)$ and $p(\cdot)$ are a pair of 1-D derivative and low-pass filters [2].

Shown in the top panel of Figure 6 is one of the 205 images with an outline around one of the $300 \times 300$ blocks. Shown in the second and third panels are, respectively, estimated blue to green warps from the entire image and from just a single block. Shown in the bottom panel is a histogram of angular errors, Equation (13), between estimates based on the entire image and those based on a single block. These errors are estimated over 50 blocks per 205 images, and over the blue to green and red to green estimates. The average angular error is 14.8 degrees with 98.0% less than 60 degrees. These results suggest that inconsistencies in block-based estimates significantly larger than 60 degrees are indicative of tampering.

Shown in the left column of Figure 7 are three original images, and in the right column are visually plausible doctored versions where a small part of each image was manipulated. For each image, the blue to green and red to green aberra-
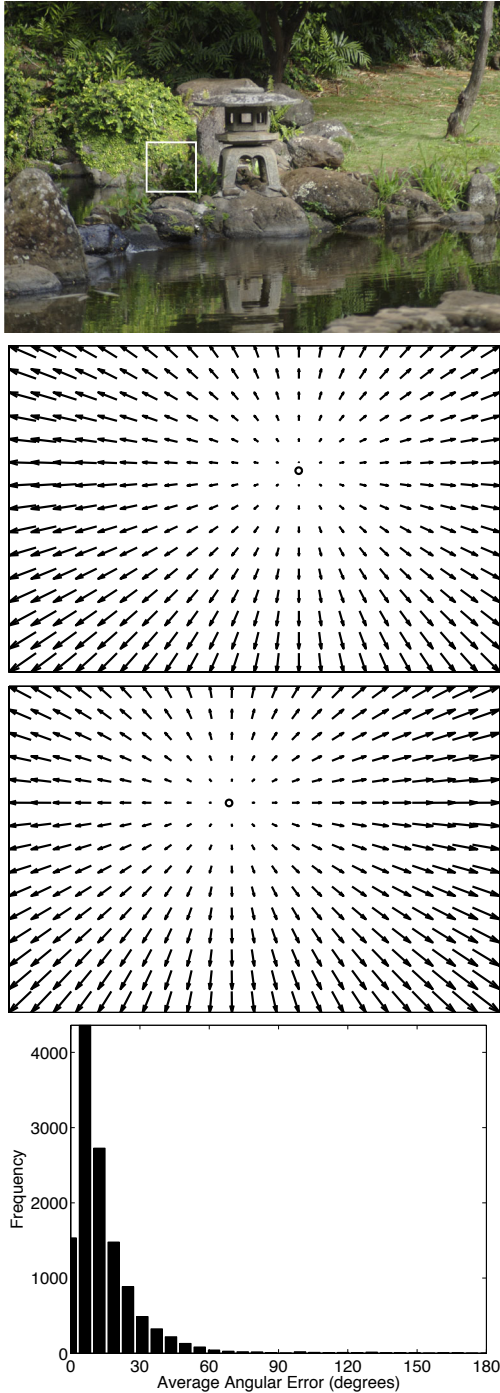
tion is estimated from the entire image. Each aberration is then estimated for all $300\times300$ blocks with an average gradient above a threshold of 2.5 gray-levels/pixel. The angular error for each block-based estimate is compared with the image-based estimate. Blocks with an average error larger than 60 degrees, and an average distortion larger than 0.15 pixels are considered to be inconsistent with the global estimate, and are used to indicate tampering. The red (dashed outline) blocks in Figure 7 reveal the traces of tampering, while the green (solid outline) blocks are consistent with the global estimate and hence authentic. For purpose of display, only a subset of all blocks are displayed.

This approach for detecting tampering is effective when the manipulated region is relatively small, allowing for a reliable global estimate. In the case when the tampering may be more significant, an alternate approach may be taken. An image, as above, can be partitioned into small blocks. An estimate of the global aberration is estimated from each block. The estimates from all such blocks are then compared for global consistency. An image is considered to be authentic if the global consistency is within an expected 60 degrees.
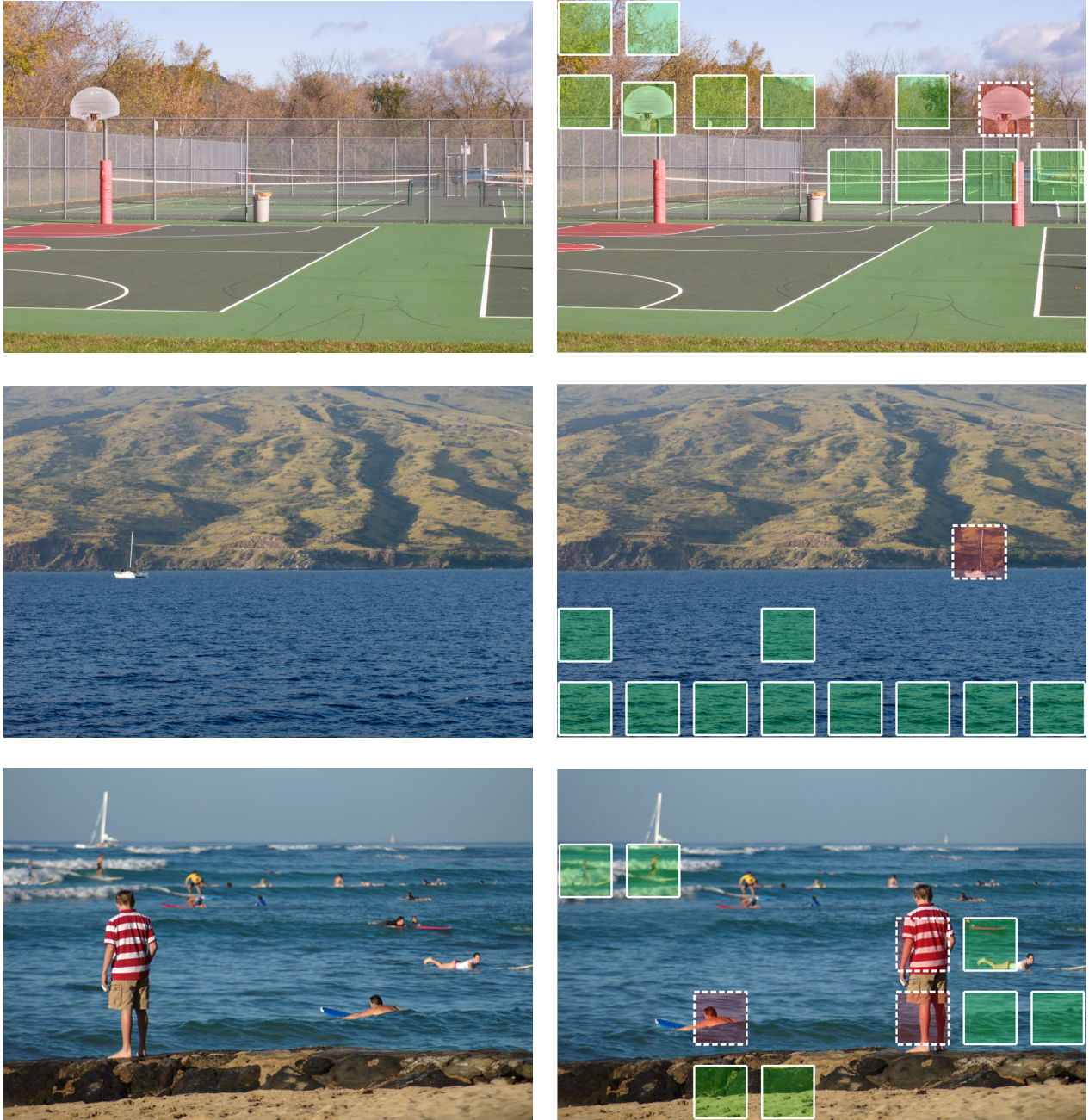
## 4. DISCUSSION

We have described a new image forensic tool that exploits imperfections in a camera's optical system. Our current approach only considers lateral chromatic aberrations. These aberrations are well approximated with a low-parameter model. We have developed an automatic technique for estimating these model parameters that is based on maximizing the mutual information between color channels (other correlation metrics may be just as effective). And, we have shown the efficacy of this approach in detecting tampering in synthetic and real images.

We expect future models to incorporate longitudinal chromatic aberrations and other forms of optical distortions. We expect that the addition of these effects will greatly improve the overall sensitivity of this approach. Since the optical aberrations from different cameras and lenses can vary widely, we also expect that the measurement of these distortions may be helpful in digital ballistics, that of identifying the camera from which an image was obtained.

## 5. ACKNOWLEDGMENTS

Figure 6: Block-based estimates. Shown are, from top to bottom, one of the 205 images with one of the $300 \times 300$ pixel blocks outlined, the estimated aberration based on the entire image, the estimated aberration based on a single block, and a histogram of 10,250 average angular errors (50 blocks from 205 images) between the image-based and block-based estimates for both the red to green and blue to green aberrations. For purposes of display, the vector fields are scaled by a factor of 150.

Figure 7: Doctored images. Shown are three original images (left) and three doctored images (right). The red (dashed outline) blocks denote regions that are inconsistent with the global aberration estimate. The green (solid outline) blocks denote regions that are consistent with the global estimate.

## Appendix A

Here we derive the 1-D and 2-D models of lateral chromatic aberration of Equations (2) and (3).

Consider in 1-D, Figure 1, where the incident light reaches the lens at an angle $\theta$, and is split into short wavelength (solid blue ray) and long wavelength (dashed red ray) light with an angle of refraction of $\theta_r$ and $\theta_b$. These rays strike the sensor at positions $x_r$ and $x_b$. The relationship between the angle of incidence and angles of refraction are given by Snell's law, Equation (1), yielding:

$$\sin(\theta) = n_r \sin(\theta_r) \tag{17}$$
$$\sin(\theta) = n_b \sin(\theta_b), \tag{18}$$

which are combined to yield:

$$n_r \sin(\theta_r) = n_b \sin(\theta_b). \tag{19}$$

Dividing both sides by $\cos(\theta_b)$ gives:

$$
\begin{aligned}
n_r \sin(\theta_r)/\cos(\theta_b) &= n_b \tan(\theta_b) \\
&= n_b x_b/f, \tag{20}
\end{aligned}
$$

where $f$ is the lens-to-sensor distance. If we assume that the differences in angles of refraction are relatively small, then $\cos(\theta_b) \approx \cos(\theta_r)$. Equation (20) then takes the form:

$$
\begin{aligned}
n_r \sin(\theta_r)/\cos(\theta_r) &\approx n_b x_b/f \\
n_r \tan(\theta_r) &\approx n_b x_b/f \\
n_r x_r/f &\approx n_b x_b/f \\
n_r x_r &\approx n_b x_b \\
x_r &\approx \alpha x_b, \tag{21}
\end{aligned}
$$

where $\alpha = n_b/n_r$.

In 2-D, an incident ray reaches the lens at angles $\theta$ and $\phi$, relative to the $x = 0$ and $y = 0$ planes, respectively. The application of Snell's law yields:

$$n_r \sin(\theta_r) = n_b \sin(\theta_b) \tag{22}$$
$$n_r \sin(\phi_r) = n_b \sin(\phi_b). \tag{23}$$

Following the above 1-D derivation yields the following 2-D model:

$$(x_r, y_r) \approx \alpha(x_b, y_b). \tag{24}$$

## 6. REFERENCES

[1] T. E. Boult and G. Wolberg. Correcting chromatic aberrations using image warping. In *Proceedings of the IEEE Conference on Computer Vision and Pattern Recognition*, pages 684–687, 1992.

[2] H. Farid and E. Simoncelli. Differentiation of multi-dimensional signals. *IEEE Transactions on Image Processing*, 13(4):496–508, 2004.

[3] J. Fridrich, D. Soukal, and J. Lukáš. Detection of copy-move forgery in digital images. In *Proceedings of DFRWS*, 2003.

[4] E. Hecht. *Optics*. Addison-Wesley Publishing Company, Inc., 4th edition, 2002.

[5] M. K. Johnson and H. Farid. Exposing digital forgeries by detecting inconsistencies in lighting. In *ACM Multimedia and Security Workshop*, New York, NY, 2005.

[6] J. Lukáš, J. Fridrich, and M. Goljan. Detecting digital image forgeries using sensor pattern noise. In *Proceedings of the SPIE*, volume 6072, 2006.

[7] T. Ng and S. Chang. A model for image splicing. In *IEEE International Conference on Image Processing*, Singapore, 2004.

[8] A. C. Popescu and H. Farid. Exposing digital forgeries by detecting duplicated image regions. Technical Report TR2004-515, Department of Computer Science, Dartmouth College, 2004.

[9] A. C. Popescu and H. Farid. Exposing digital forgeries by detecting traces of resampling. *IEEE Transactions on Signal Processing*, 53(2):758–767, 2005.

[10] A. C. Popescu and H. Farid. Exposing digital forgeries in color filter array interpolated images. *IEEE Transactions on Signal Processing*, 53(10):3948–3959, 2005.

[11] P. Viola and W. M. Wells, III. Alignment by maximization of mutual information. *International Journal of Computer Vision*, 24(2):137–154, 1997.

[12] R. G. Willson and S. A. Shafer. What is the center of the image? *Journal of the Optical Society of America A*, 11(11):2946–2955, November 1994.